Thermophysics and Aeromechanics, *2024*, *Vol. 31*, *No. 2*

DOI: 10.1134/S0869864324020094

Modeling shock-wave cells at the initial region of the underexpanded supersonic jet

I.A. Shirokov[1] and T.G. Elizarova[2]

[1]*Lomonosov Moscow State University*, *Moscow*, *Russia*

[2]*Keldysh Institute of Applied Mathematics RAS*, *Moscow*, *Russia*

E-mail: ivanshirokov@inbox.ru

(*Received June 30*, *2023*; *revised August 9*, *2023*;
accepted for publication November 21, *2023*)

Supersonic underexpanded air jet modeling based on the QGD algorithm is carried out. The process of jet flow evolution and the formation of unsteady flow regions are investigated to obtain a good qualitative and quantitative agreement of the results with experimental and simulation data, known from the literature. The QGD algorithm is shown to enable studies of the structure of shock-wave cells at the initial region of the flow and to describe the general character of the turbulent jet.

Keywords: quasi-gas-dynamic (QGD) equations, jet flow, shock-wave cells

Introduction

The research into jet gas flows is of great significance for promising developments in the field of engine manufacturing. The experimental study of jets is widespread but quite cost-intensive and unfeasible for many tasks that are interesting from a practical point of view. In this regard, the elaboration and validation of methods for computer modeling of jet streams become important.

Works [1, 2] present experimental results, obtained under laboratory conditions in the study of the outflow of air jets with various parameters into the region of stationary air under normal conditions. The axial pressure profiles and Mach numbers given in these papers can serve as reference data for validation of computer modeling methods. Along with this, the experiments reveal about ten shock wave cells ("barrels") that occur during jet flows in off-design regimes (when the pressure at the nozzle section does not correspond to external pressure). The difficulty of numerical modelig of such flows is that difference algorithms often do not resolve the experimentally observed number of "barrels" in a highly unsteady flow.

Works [3, 4] were also devoted to experimental studies of transonic and supersonic underexpanded air jets. At that, three-dimensional distributions of density [3], temperature and average velocity [4] were studied and visualized. The parameters of the jets studied by the authors in [3, 4] differ from those in [1, 2]. In particular, in [4], in contrast to [1– 3], jet heating was used.

There are numerous papers on numerical modeling of jet streams using a variety of computational approaches, a complete review of which seems impossible. Some of them are mentioned in the list of references (see, e.g., [5 – 7]). Nevertheless, an analysis of well-known publications shows that in calculations, the available algorithms do not allow obtaining a large number of "barrels", which is observed in some experiments. There may be several reasons for this: too high or inadequate scheme viscosity and non-stationary or turbulent effects in the jet, the modeling of which requires fine-tuning of turbulence models, used in the calculation, or accurate modeling of the unsteady behavior of the entire jet as a whole.

In [5], a supersonic jet was simulated on the grounds of experimental data of [1], which served as the basis for the formulation of the problem in this work. The authors of [5] used the higher-order Godunov method to solve the averaged Navier–Stokes equations in conjunction with various turbulence models. It was found that the axial pressure profiles in the near zone (the first 4 – 5 "barrels") well agree with the experimental profiles (although the amplitude of the profile oscillations is less than the experimental amplitude even in the first "barrels"), and at a distance from the nozzle, both the amplitude and frequency show values noticeably less than the experimental ones. In [6] (p. 104), an underexpanded jet was also modeled by solving the averaged Navier–Stokes equations jointly with SST and SA turbulence models, and then the results were compared with experimental data of [1]. The obtained data were, in general, consistent with those of the calculations [5] and experimental data. Thus, a special adjustment of the turbulence models provided a relatively good agreement of the results of [5] and [6] with experimental data, although high accuracy of modeling of a large number of "barrels" has not been achieved.

In [7], an underexpanded jet was modeled in a formulation based on experimental data of [8]. The Russian VP2/3 software package, including the implementation of the method of splitting with respect to physical processes within the framework of a generalized pressure correction procedure, was used. A very good agreement between the transverse profiles and the experimental results was obtained [8], and the flow pattern, including the features of turbulent zones, was studied in detail. This work did not aim at modeling a large number of "barrels".

This paper employs a numerical algorithm based on regularized (or quasi-gas-dynamic (QGD)) equations to simulate shock wave cells arising in an underexpanded supersonic jet [9 –12]. The goal of the work is to test the application of the QGD algorithm to this class of problems, since it has been successfully used to calculate underexpanded jets (including nonequilibrium effects) earlier (see, e.g., [13]). At the same time, the problem of obtaining a large number of "barrels" was not emphasized. In addition, the QGD model has a built-in turbulence model, the role of which in jet calculation tasks requires research. Examples of the use of the QGD algorithm for calculating turbulent flows may be found in [10, 12 – 17].

In [18], the QGD model was for the first time generalized to the case of a multicomponent gas flow, taking into account translational-vibrational disequilibrium. The numerical algorithm constructed in [18] was used to calculate supersonic off-design jets of moderately rarefied gas and analyze their thermal radiation. The application of the QGD equations was found to more accurately reflect the thermal properties of the jet. In particular, the radiation intensity turns out to be significantly lower than when calculated on the basis of the Navier–Stokes equation system, since the translational, rotational and vibrational temperatures decrease in the mixing layer.

Problem statement

The problem of the jet flow modeling corresponds to one of the variants of the experimental formulation described in [1, 2] and is considered in a three-dimensional formulation

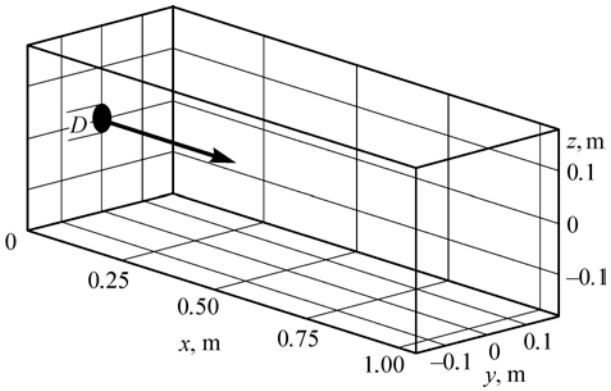

Fig. 1. Scheme of the computational domain.

in Cartesian coordinates. A circular gas jet flows into an area shaped like a rectangular parallelepiped (Fig. 1) filled with a stationary gas under normal conditions. The jet parameters are selected in accordance with the experimental work [1]. The jet diameter at the inlet is D = = 0.0508 m. The gas is considered ideal, and its equation of state relates pressure, density and temperature as follows: $p = \rho RT$. The parameters correspond to air parameters: the adiabatic constant is $\gamma = 1.4$, the gas constant is $R = 287$ J/(kg·K), and the Prandtl number is Pr = 0.737.

The jet parameters in experiments [1, 2] are determined by the following values: the Mach number at the nozzle section Ma (determined by the nozzle shape) and the parameter β, associated with the ideal Mach number of a fully expanded jet (i.e., jets in the design mode when the pressure at the nozzle section is atmospheric) Ma_j by the dependence $\beta = \left((\mathrm{Ma}_j)^2 - 1\right)^{1/2}$. This paper considers the flow with Ma = 2, $\beta = 2$ (with $\mathrm{Ma}_j = 2.236$). For modeling, it is required to know not only Ma, but also the density and pressure at the nozzle section. Let us calculate these values as follows.

In the undisturbed region, density, pressure and temperature are assumed to be determined by normal atmospheric conditions: $\rho_1 = 1.20433$ kg/m^3, $p_1 = 101325$ Pa, and $T_1 = 293.15$ K. Considering the jet in the design mode and assuming that at the nozzle section Ma = Ma_j and $p = p_1$, we calculate the stagnation pressure based on the isentropic formula [19] (p. 108). Since jet heating was not used in [1, 2], we assume that the stagnation temperature equals T_1. Knowing the stagnation parameters and the Mach number Ma at the nozzle section, we determine the pressure (p_0 = 146495Pa) and temperature (T_0 = 162.861 K) using the isentropic formulas [19]. With the equation of state, we find the density at the nozzle section — $\rho_0 = 3.13418$ kg/m^3. The speed of sound in this case is $c_0 = (\gamma RT_0)^{1/2} = 255.808$ m/s. Thus, the degree of the jet off-design is $p_0/p_1 = 1.46$.

Mathematical model

Modeling of the supersonic jet flow of viscous gas was carried out on the basis of a system of quasi-gasdynamic equations for an ideal polytropic gas, constructed in [9–11]. The QGD regularization is based on the fact that the mass density of the flow $\mathbf{j}_m$ differs from the momentum of a unit volume of gas $\rho\mathbf{u}$, leading to the appearance of small additional dissipative terms in each of the equations of the system. These regularizing terms have a physical character and improve the numerical stability properties of explicit difference algorithms in which spatial derivatives are approximated by central differences.

In Cartesian coordinates, in the absence of external forces and heat sources, the QGD system is written as:

$$\frac{\partial}{\partial t}\rho + \nabla_i j_m^i = 0, \tag{1}$$

$$\frac{\partial}{\partial t}\rho u^j + \nabla_i \left(j_m^i u^j \right) + \nabla^j p = \nabla_i \Pi^{ij}, \tag{2}$$

$$\frac{\partial}{\partial t}E + \nabla_i \left(j_m^i H \right) + \nabla_i q^i = \nabla_i \left(\Pi^{ij} u_j \right), \tag{3}$$

where u_i are the components of the macroscopic velocity, $E = \rho u^2/2 + p/(\gamma - 1)$ is the total specific energy, and $H = (E + p)/\rho$ is the total specific enthalpy. The expressions for the vector of the mass flux density j_m^i, the viscous stress tensor Π^{ij} and the heat flux q^i are written as

$$j_m^i = \rho\left(u^i - w^i\right), \;\; w^i = \frac{\tau}{\rho}\left(\nabla_j \rho u^i u^j + \nabla^i p\right), \tag{4}$$

$$\Pi^{ij} = \Pi_{\mathrm{NS}}^{ij} + \tau u^i \rho\left(u_k \nabla^k u^j + \frac{1}{\rho}\nabla_j p \right) + \tau \delta^{ij}\left(u_k \nabla^k p + \gamma p \nabla^k u_k \right), \tag{5}$$

$$\Pi_{\mathrm{NS}}^{ij} = \mu\left(\nabla^i u^j + \nabla^j u^i - \frac{2}{3}\delta^{ij}\nabla^k u_k \right) + \xi \delta^{ij}\nabla^k u_k, \tag{6}$$

$$q^i = q_{\mathrm{NS}}^i - \tau u^i \rho\left(u_j \nabla^j \varepsilon + p u_j \nabla^j \frac{1}{\rho} \right), \quad q_{\mathrm{NS}}^i = -\kappa \nabla^i T, \tag{7}$$

here $\varepsilon = p/\left(\rho(\gamma - 1)\right)$ is the internal energy of a unit mass of a gas, Π_{NS}^{ij} and q_{NS}^i are the viscous stress tensor and heat flux in the Navier–Stokes system, μ, ξ and κ are the coefficients of shear and bulk viscosity and thermal conductivity, respectively. Let us define μ through the temperature dependence:

$$\mu = \mu_0 \left(T / T_0 \right)^{\omega}, \tag{8}$$

where $\mu_0 = 1.16869 \cdot 10^{-5}$ kg/(m·s) is the viscosity of the gas at a temperature at the nozzle section T_0 (the viscosity value was obtained based on data for the standard atmosphere at an altitude of 4160 m, GOST (SS) 4401-81), and $\omega = 0.74$ is the exponent of intermolecular interaction. Let us express the coefficient of thermal conductivity using the Prandtl number Pr:

$$\kappa = \mu R\gamma / \left(\mathrm{Pr}(\gamma - 1)\right), \tag{9}$$

the bulk viscosity coefficient is set to zero. The Reynolds number, calculated from the initial viscosity μ_0, nozzle size D, initial velocity $\mathrm{Ma} \cdot c_0$ and initial density ρ_0, is $\mathrm{Re} = 7 \cdot 10^6$.

The coefficient τ, which determines the additional dissipation in the QGD algorithm, for a viscous polytropic gas has the order of the free time between collisions of gas particles. In the performed calculations, its value is associated with the step of the spatial grid h:

$$\tau = \alpha h / c, \tag{10}$$

where c is the local speed of sound and $\alpha = 0.6$–1.0 is the adjustment parameter.

Computational grids and numerical solution method

In the computational domain (Fig. 1) let us introduce a uniform grid with cubic cells. A circular nozzle with a diameter D is placed on the wall ($x = 0$) and is located symmetrically relative to the Y and Z axes. The dimensions of the computational domain in the Y and Z directions are the same and equal to $7D$. The length of the computational domain in the X direction in different versions is $21D$ and $35D$. Depending on the size of the grid, 10, 20, and 30 of cells account for the nozzle diameter. Four grid variants are used in the work, their characteristics being shown in the table.

On the constructed grids, the QGD equations are approximated by central differences, and the approximation has the second order of accuracy in space. The solution of the initial boundary value problem for the grid analogues of the QGD equations (1) – (7), taking into account the ratios (8) – (10), is found according to an explicit finite difference scheme with the first order approximation in time. The time step is calculated as $h_t = \beta_C h/c_0$, where $\beta_C = 0.01–0.02$ is the Courant number.

At the initial moment, the nozzle section parameters ρ_0, p_0, T_0 and the horizontal velocity $\mathrm{Ma}\cdot c_0$ are set in a horizontal cylinder with a base coinciding with the nozzle on the wall ($x = 0$) and occupying the entire length of the computational domain. The parameters of the undisturbed gas are set outside the cylinder (normal conditions at ρ_1, p_1, T_1 and zero velocity). During calculation according to an explicit scheme, the gas parameters are kept constant at the nozzle section at $x = 0$, and the parameters of the undisturbed gas are maintained constant outside the nozzle on the wall ($x = 0$). At the remaining boundaries of the domain, all normal derivatives are kept equal to zero. Although such conditions correspond to fully supersonic flow, when calculating an underexpanded supersonic jet flowing into a region of stationary gas, they also work well, despite the presence of subsonic regions outside the jet.

The calculations were carried out using a K-100 supercomputer installed in the Center of Collective Use of the M.V. Keldysh Institute of Applied Mathematics of the Russian Academy of Sciences [20]. The parallel computations technique was used based on the decomposition of the computational domain, using the MPI standard. Depending on the calculation option, the machine time ranged from 30 minutes to 20 hours when using 96 to 128 processor cores.

It should be noted that the application of the described numerical algorithm for the QGD equations in the problem of modeling the Taylor-Green vortex decay [14] provided a good agreement of the kinetic energy dissipation profile with the reference data, as well as the correspondence of the energy spectrum to the Kolmogorov law of decreasing energy with increasing frequency in the inertial interval. In these calculations the step of the spatial grid ranged from 0.0005 to 0.00025 m and the adjustment parameter α varied from 0.1 to 1. The application of the same algorithm for the QGD equations in modeling the turbulent Couette flow in a flat channel [15] has shown a good agreement of the values of turbulent pulsations of three components of the flow velocity with the corresponding experimental and calculated data, known

Table

Variants of computational grids

Grid	Length of the domain	Cells per diameter, CPD	Grid step h, m	Number of grid nodes
1	$21D$	10	0.005	1088640
2	$21D$	20	0.0025	8468880
3	$21D$	30	0.0017	28314720
4	$35D$	10	0.005	1814400

from the literature, with the grid step being 0.001 m and the parameter $\alpha = 0.1$. In [21] the QGD algorithm implemented in the OpenFOAM software package was used to simulate the interaction of strongly underexpanded gas jets with obstacles. A good agreement was obtained between the calculated and experimental data in modeling complex shock wave cells arising from such interaction.

The evolution of the jet stream and the choice of averaging time

The analysis of the jet stream development over time, carried out using modeling at $\alpha = 0.8$ and $\alpha = 1.0$ on different computational grids with an area length of $35D$, demonstrates qualitatively similar results. Figure 2 shows the calculated instantaneous pressure levels in the section $z = 0$ for time points 2, 4, 30, and 50 ms, as well as the pressure levels averaged from 30 to 50 ms obtained on the grid 4 at $\alpha = 0.8$.

The evolution of the jet stream occurs as follows. From the initial moment to 2 ms, a periodic structure is formed in the near zone of the jet ($x < 20D \sim 1$ m, 6 – 7 "barrels"). After that, the periodic structure in this zone changes little.

In the time period from 4 to 30 ms, a transient process of formation of an unsteady flow occurs in the region of $20D < x < 35D \approx 1.75$ m, and from 30 to 50 ms, the jet flow in this region becomes markedly turbulent. The general structure of the flow in the period from 30 to 50 ms remains, while the flow becomes asymmetric. In the area $x < 20D$, 6 – 7 relatively stable "barrels" with non-stationary vortex structures present around them continue to exist. In the area of $20D < x < 35D$, there is a generally non-stationary part of the flow, but several "barrels"

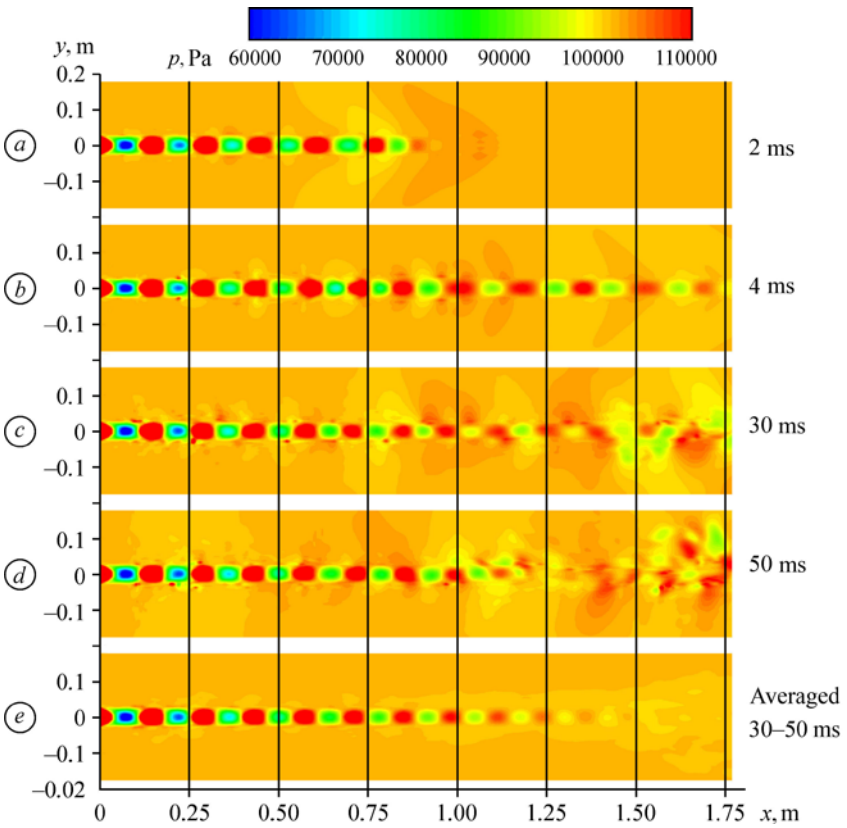

Fig. 2. Instantaneous (*a* – *d*) and averaged from 30 to 50 ms (*e*) pressure levels in section $z = 0$.

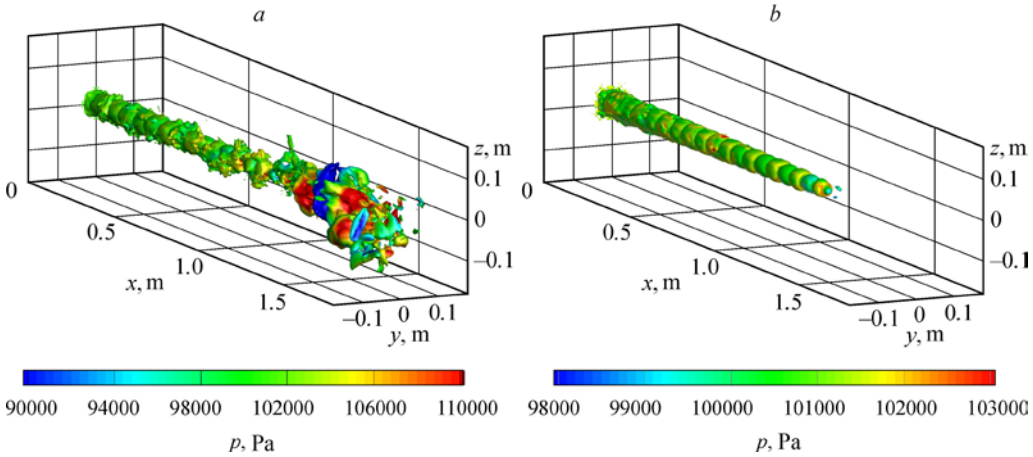

Fig. 3. Instantaneous (*a*) and averaged from 30 to 44 ms (*b*) pressure levels plotted on the isosurface of the pressure gradient module at a time of 44 ms.

(albeit weakly expressed) exist in this area, as can be seen in the pressure field averaged from 30 to 50 ms (Fig. 2*e*). The general character of the jet is turbulent, which corresponds to the Reynolds number calculated from the initial parameters of the jet. The character of the averaged periodic structures in this case corresponds to the experimental data of [1, 2] for the considered jet variant. Averaging the simulation data before comparing with the experimental results is justified, since, as the authors of [1] indicate, the experimental data are also averaged over time, and pulsations are not investigated.

To illustrate the three-dimensional asymmetric nature of the unsteady jet flow, Figure 3 shows the pressure levels plotted on the isosurface of the pressure gradient at a time of 44 ms in an unaveraged and averaged form, obtained by modeling on a grid 4 at $\alpha = 0.8$.

Figure 4 demonstrates with a solid line a spectrum of the specific kinetic energy of a non-stationary section of the jet, corresponding to Fig. 3*a*, at 44 ms (grid 4, $\alpha = 0.8$). The spectrum was calculated in a cubic region close to the output boundary ($1.4 < x < 1.67$, $-0.13 < y < 0.13$, $-0.13 < z < 0.13$ m) via the non-averaged flow field. The method of calculating the energy spectrum is based on the discrete Fourier transform and described in detail in [16]. Figure 4 also shows a dashed line with an angular coefficient of –5/3, corresponding to Kolmogorov's law of decreasing energy of turbulent pulsations with increasing frequency. It can be seen that the numerical method used in this work and the selected dimensions of the computational cells allow modeling the spectrum of pulsations on a part of the inertial interval, as in the cases of applying the QGD algorithm to the problems of modeling the decay of a Taylor–Green vortex [14] and that of homogeneous isotropic turbulence [16].

The analysis of the evolution of the jet stream shows that to study the near zone of the flow, it is sufficient to perform modeling at the length of the region 21*D* (grids 1, 2 and 3) and to average from 2 to 4 ms. To study

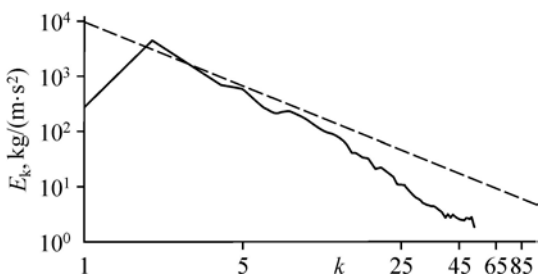

Fig. 4. The specific kinetic energy spectrum of the turbulent jet zone at 44 ms (solid curve) and a straight line with an angular coefficient of –5/3, corresponding to the Kolmogorov law of decreasing energy of turbulent pulsations (dashed line).

the features of the non-stationary jet region far from the nozzle, it is required to use a longer computational domain and a longer calculation time, averaging, for example, from 30 to 50 ms. However, it becomes difficult to use detailed grids (from 20 or more cells per D), since the machine calculation time greatly increases.

Note that a gas particle at the speed of sound would have managed to travel about 1 m for the time of 4 ms, which is approximately equal to the length of the calculated region $21D$. When studying nonstationary regions in a jet stream, it is advisable not to apply symmetry conditions during modeling, since such a flow has a significantly three-dimensional asymmetric character. In addition, when modeling asymmetric structures, it is preferable to use a uniform grid with cubic cells.

Convergence of results at mesh refinement

Figure 5 shows the axial profiles of the average pressure normalized to atmospheric pressure p_{atm}. Symbols *1* correspond to the experimental results of work [1], curves *2 – 4* represent the results of modeling based on the QGD algorithm on grids 1 (curve *2*), 2 (curve *3*) and 3 (curve *4*). The length of the region is $21D$, the tuning parameter $\alpha = 0.6$, and averaging was carried out from 2 to 4 ms. The full computational domain is illustrated on the left, and the fragment containing the first three "barrels" is on the right. It can be seen that at mesh refinement, the simulation results become noticeably closer to the experimental data. The insufficient (compared with experimental values) amplitude of oscillations in the pressure profile in the calculation is probably due to the dissipativity of the used variant of the QGD algorithm, which ensures the stability of the calculation when modeling the flow of a complex structure in the presence of supersonic and subsonic regions, as well as turbulence zones. Nevertheless, the results obtained on grids 2 and 3 show, in general, quite good agreement with experimental data, in particular, on grid 3 it is possible to resolve the stepwise character of the profile of the first two "barrels". Perhaps, using more detailed grids based on the QGD algorithm, a more accurate correspondence of the maximum values to the experimental data may be obtained. At $x > 10D$, the frequency and amplitude of periodic structures lag behind the experimental values, but at the same time, the data of the fine grid are, in general, closer to the experimental values than those obtained on coarser ones.

Figure 6 shows the axial profiles for the averaged Mach number, while the calculation parameters and designations here are the same as in Fig. 5. The analysis of the figure also demonstrates the convergence of the results to experimental data at mesh refinement and

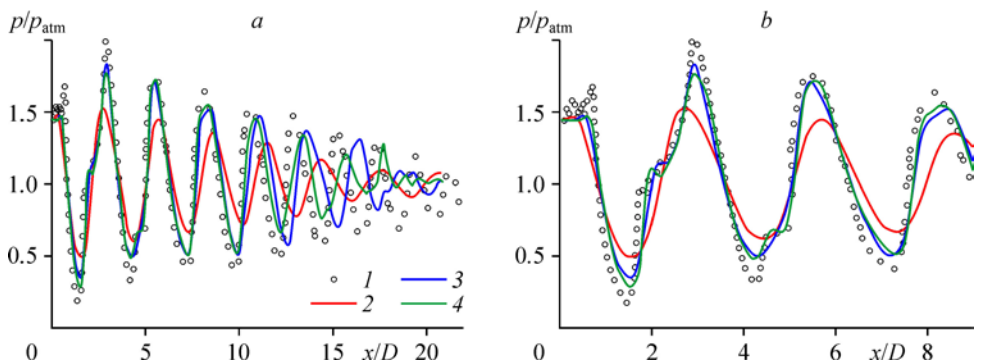

Fig. 5. Axial profiles of the averaged normalized pressure.

1 — experimental data [1],

2 – 4 – simulation results based on the QGD algorithm for CPD = 10 (*2*), 20 (*3*), 30 (*4*).

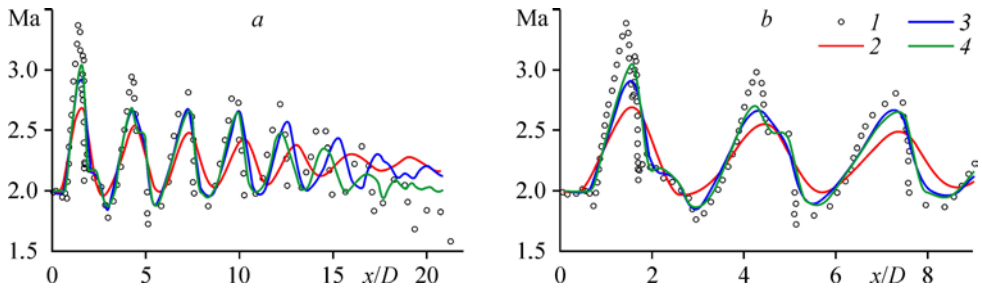

Fig. 6. Profiles of the average Mach number.
See the designations in Fig. 5.

a good quantitative correspondence to the experiment at $x < 10D$, including the presence of steps in the Mach number profile in the first and second "barrels". However, for the Mach number, the lower value of the amplitude of the profile oscillations in comparison with the experimental data is more noticeable than for pressure, and the steep fronts of the experimental profile are somewhat smeared.

The frequency discrepancy with the experimental data is observed in the area far from the nozzle: according to the calculation results, the "barrels" are located slightly further from the nozzle compared to the experimental data. The authors of [1] claim that during laboratory experiments, a boundary layer development occurs in the expanding part of the supersonic nozzle. Perhaps, this leads to a decrease in the effective diameter of the nozzle, so the scale of the x/D coordinate is not precisely determined. On the other hand, the effective diameter of the nozzle is not accurately determined in the calculation either, due to the approximation of the nozzle on the calculated grid with square cells, especially when using coarser grids. Therefore, the scales of the abscissa axis might not match when constructing experimental and calculated axial profiles, and in this case, comparing the location of the "barrels" at a distance from the nozzle is not very indicative.

The dependence of the results on the adjustment parameter of the QGD algorithm

Figure 7 shows the axial profiles of the average pressure normalized to atmospheric pressure p_{atm}. Symbols *1* correspond to the experimental results of [1], curves *2*–*4* show the simulation results for different values of the adjustment parameter of the QGD algorithm: $\alpha = 1.0$ (curve *2*), $\alpha = 0.8$ (curve *3*) and $\alpha = 0.6$ (curve *4*). The length of the area is $21D$,

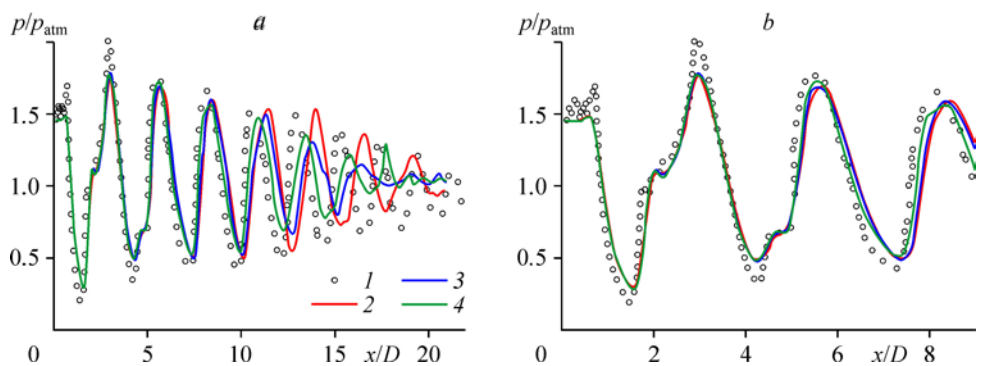

Fig. 7. Axial profiles of the averaged normalized pressure.
1 — experimental data [1], *2*–*4* — calculation results for $\alpha = 1$ (*2*), 0.8 (*3*), 0.6 (*4*).

a grid 3 is used, and averaging is carried out from 2 to 4 ms. The full computational domain is on the left, and the fragment containing the first three "barrels" is shown on the right. Figure 7 demonstrates that with a decrease in α, the simulation results become somewhat closer to the experimental data, especially at $x > 10D$, although in this area all the calculation results lag behind the experimental ones in frequency and amplitude. At $x < 10D$, the calculation results depend little on α and are very close to experimental data.

Conclusion

Modeling of a supersonic underexpanded submerged jet, carried out on the basis of the QGD algorithm in a three-dimensional formulation, allows determining the structure of periodic shock wave regions ("barrels"), as well as the general structure of the flow and the spectrum of turbulent pulsations of the unsteady flow zone in part of the inertial interval. At the use of computational grids containing about 30 cells per the jet diameter, a fairly good quantitative agreement with experimental data in the near zone of the jet (the first 3–4 "barrels") has been obtained. It is preferable to use more detailed grids (there is a convergence of the results to experimental values at the grid refinement) and lower values of the adjustment parameter of the QGD algorithm ($\alpha = 0.6$ compared to 1.0). However, even when using relatively coarse grids (10 cells per jet diameter), the formation of about ten "barrels" is detected on quite long computational domain, as in the experiment.

The authors are grateful to M.V. Kraposhin and A.S. Epikhin for discussing the problem under study.

References

1. **J.M. Seiner and T.D. Norum,** Experiments of shock associated noise on supersonic jets, AIAA Paper, 1979, No. 79–1526.
2. **T.D. Norum and J.M. Seiner,** Measurements of mean static pressure and far-field acoustics of shock-containing supersonic jets, NASA Technical Memorandum 84521, 1982.
3. **O. Leon, D. Donjat, F. Olchewsky, J. Desse, F. Nicolas, and F. Champagnat,** Three-dimensional density field of a screeching under-expanded jet in helical mode using multi-view digital holographic interferometry, J. Fluid Mech., 2022, Vol. 947, P. A36-1–A36-38.
4. **J. McGuirk and T. Feng,** The near-field aerodynamic characteristics of hot high-speed jets, J. Fluid Mech., 2021, Vol. 915, P. A120-1– A120-31.
5. **G.S. Glushko, I.E. Ivanov, and I.A. Kryukov,** Turbulence modeling for supersonic jet flows, Physical-Chemical Kinetics in Gas Dynamics, 2010, Vol. 9, P. 142-1–142-8. http://chemphys.edu.ru/issues/2010-9/articles/142/
6. **N.F. Kudimov, A.V. Safronov, and O.N. Tretyakova,** Applied Problems of Gas Dynamics and Heat Transfer in Power Engines of Rocket Technology. MAI Publ., Moscow, 2014.
7. **S.A. Isaev, Y.M. Lipnitskii, P.A. Baranov et al.,** Simulation of a turbulent supersonic underexpanded jet flowing into a submerged space with the help of a shear stress transfer model, J. Eng. Phys. Thermophys., 2012, Vol. 85, P. 1357–1371.
8. **V.I. Zapryagaev, I.N. Kavun, and N.P. Kiselev,** Flow structure at the initial section of a supersonic jet exhausting from a nozzle with chevrons, J. Appl. Mech. Tech. Phys., 2010, Vol. 51, P. 202–210.
9. **B.N. Chetverushkin,** Kinetic Schemes and Quasi-Gas Dynamic System of Equations, CIMNE, Barselona, 2008.
10. **T.G. Elizarova,** Quasi-Gas Dynamic Equations, Springer, Dordrecht, 2009.
11. **Yu.V. Sheretov,** Regularized Hydrodynamic Equations, Tver State University, Tver, 2016.
12. **T.G. Elizarova and I.A. Shirokov,** QGD Equations and Examples of Applications in Gas Dynamic Flow Simulation, MAKS Press, Moscow, 2017.
13. **B. Mate, I. Graur, T. Elizarova, I. Chirokov, G. Tejeda, J. Fernandez, and S. Montero,** Experimental and numerical investigation of an axisymmetric supersonic jet, J. Fluid Mech., 2001, Vol. 426, P. 177–197.
14. **I.A. Shirokov and T.G. Elizarova,** Simulation of laminar–turbulent transition in compressible Taylor–Green flow basing on quasi-gas dynamic equations, J. Turbulence, 2014, Vol. 15, Iss. 10, P. 707–730.
15. **I.A. Shirokov and T.G. Elizarova,** Application of quasi-gas dynamic equations to numerical simulation of near-wall turbulent flows, Comp. Math. Model., 2017, Vol. 27, Iss. 1, P. 37–59.

16. T.G. Elizarova and I.A. Shirokov, Testing of the QGD-algorithm by a Homogeneous Isotropic Gas-Dynamic Turbulence Decay, KIAM Preprint No. 35, Moscow, 2013.

17. I.A. Shirokov and T.G. Elizarova, Modeling of unsteady subsonic flow around an axisymmetric body with a turbulator, Thermophysics and Aeromechanics, 2022, Vol. 29, No. 1, P. 35–42.

18. A.M. Molchanov and V.E. Popov, Calculation of gas dynamics and radiation of high-altitude jets, Physical-Chemical Kinetics in Gas Dynamics. 2018. V.19, Iss. 2, P. 753-1–753-20. http://chemphys.edu.ru/issues/2018-19-2/articles/753/

19. L.G. Loitsianskii, Mechanics of Liquids and Gases, Pergamon Press, New York, 1966.

20. K-100 System, Keldysh Institute of Applied Mathematics RAS, Moscow. https://www.kiam.ru/MVS/resourses/k100.html (access date: 31.05.2024)

21. A.S. Epikhin and T.G. Elizarova, Numerical simulation of underexpanded supersonic jets impingement on an inclined flat plate, Thermophysics and Aeromechanics, 2021, Vol. 28, No 4, P. 479–486.